PROCEEDINGS OF SCIENCE

^{26}Al Gamma-ray Line Emission From Solar System Bodies

PoS(ICRC2023)680

Tatsuki Fujiwara[a,*] **and Yoshiyuki Inoue**[a,b]

[a] *Department of Earth and Space Science, Graduate School of Science, Osaka University,*
Toyonaka, Osaka 560-0043, Japan

[b] *University, Department,*
Street number, City, Country

E-mail: `fujiwara@astro-osaka.jp`, `yinoue@astro-osaka.jp`

In the Solar system, the radioisotope ^{26}Al exists on the surface of celestial bodies due to the nuclear spallation by low-energy cosmic rays. Meteorites sampled on the Earth and lunar samples allow us to measure their current decay rate in laboratories. Based on those reported ^{26}Al decay rate, in this presentation, we report the expected ^{26}Al gamma-ray line signals from solar system bodies, especially asteroids in the main belt and the Moon. We find that the signals from the main belt are too weak for future coming MeV gamma-ray missions. However, due to its proximity and mass, the next generation MeV gamma-ray mission such as the Compton Spectrometer and Imager (COSI) satellite will be able to see the ^{26}Al signals from the moon. The future ^{26}Al measurement will help us to understand lunar geology.

38th International Cosmic Ray Conference (ICRC2023)
26 July - 3 August, 2023
Nagoya, Japan

---

[*] Speaker

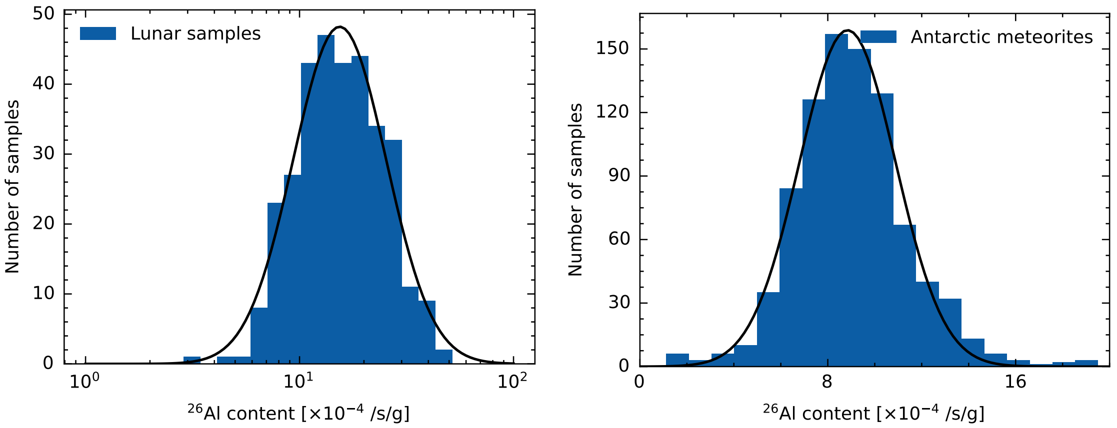

(a) (b)

Figure 1: ^{26}Al content (decay rate) for 1(a): lunar samples, and for 1(b): antarctic meteorites of asteroid origin, respectively. The units [/s/g] show ^{26}Al decay rate per unit sample mass. Solid lines of 1(a) and 1(b) show these fittings by the log-normal distribution and the normal distribution, respectively. These data are taken from [2], [3] and references therein.

1. Introduction

2. Methods and Results

2.1 Experimental measurements of Aluminium-26 content in meteorites

Meteorites of asteroid origin sampled on Earth and lunar samples collected by the Apollo program contain ^{26}Al (See, Section 1). These meteorite samples allow us to measure ^{26}Al current decay rate in laboratories (e.g., [1]) . Figure 1 shows ^{26}Al content (decay rate) of these measured samples ([2], [3] and references therein). Figure 1(a) and 1(b) represent ^{26}Al decay rate of lunar samples and that of meteorites of asteroid origin sampled in the Antarctic, respectively. The units of ^{26}Al content of [/s/g] show ^{26}Al decay rate per unit sample mass. We can see from the black solid lines in Figure 1 that lunar samples and antarctic meteorite samples are approximated to the log-normal distribution and the normal distribution, respectively. The expectation values from these fittings are 2.2×10^{-3} /s/g for lunar samples and 8.8×10^{-4} /s/g for antarctic meteorites.

In this research, we assume that ^{26}Al content for lunar samples of 2.2×10^{-3} /s/g and that for meteorites of 8.8×10^{-4} /s/g are the typical values for the Moon and all the MBAs (hereafter $\epsilon_{☾}$ and ϵ_{MBA}) respectively. In addition to this, we presume that each celestial body has the ^{26}Al content uniformly on its surface throughout the discussion below. Therefore, based on these assumptions, once we determine a CR interacting domain with celestial matters, we can obtain the total 1.8 MeV photon production rate of those celestial bodies since 26Al is produced through nuclear spallation by low-energy CRs.

PoS(ICRC2023)680

2.2 Aluminium-26 gamma-ray flux from the Moon

In this research, we treat the Moon as a perfect sphere with a radius $R_{\leftmoon}$ of 1.737×10^8 cm[1] [4] and with a uniform density distribution on its surface for simplicity.

To derive the CR bombarding region on the Moon, we evaluated a CR penetration length Δr as a mean free path of CR protons through inelastic collisions with matter of the lunar surface:

$$\Delta r = \frac{1}{\int_{10\,\mathrm{MeV}}^{200\,\mathrm{MeV}} I_\mathrm{p}(E)\mathrm{d}E} \int_{10\,\mathrm{MeV}}^{200\,\mathrm{MeV}} \mathrm{d}E \left(\sum_i n_i \sigma_{i\mathrm{p}}(E) \right)^{-1} I_\mathrm{p}(E), \tag{1}$$

where n_i is the number density of element i on its surface, $\sigma_{i\mathrm{p}}(E)$ is the inelastic cross section of element i with injected protons with kinetic energy E, and $I_\mathrm{p}(E)$ is CR proton intensity. Using lunar chemical composition and its mass density $\rho_{\leftmoon} = 3.01\,\mathrm{g/cm^3}$ [5], we estimated the number density n_i (i = O, Na, Mg, Al, Si, Ca, Ti, Fe)[2] . We collected the cross-section data $\sigma_{i\mathrm{p}}(E)$ using TALYS nuclear reaction code [8]. TALYS can calculate the cross section up to 200 MeV of a injected particle energy. Since these inelastic cross section have peak at from a few tenth to a few hundreds MeV, we took the mean among the range as in Eq.(1). We determined CR proton spectrum in this energy range by power-law fitting: $I_\mathrm{p}(E) \propto E^{0.836}$. As a result, we obtained $\Delta r \simeq 33$ cm. Since $\Delta r \ll R_{\leftmoon}$, we can treat the ^{26}Al contained region as a spherical shell which has a volume of $4\pi R_{\leftmoon}^2 \Delta r$.

Before deriving ^{26}Al photon production rate, we should note that 1.8 MeV photons interact with matter in the lunar interior. From sub-MeV to a few MeV domain, gamma-ray interactions with matter are dominated by the Compton scattering (e.g., [9]). In this research, we solely consider this process for photon-matter interactions. Since we are interested in photon energy only at 1.8 MeV, we can regard this process as the 'self absorption' with the absorption coefficient α of $[\sigma_{\mathrm{KN}<1.8>} \sum_i Z_i n_i]$, where $\sigma_{\mathrm{KN}<1.8>}$ is the Klien-Nishina cross section which gamma-ray energy of 1.8 MeV (e.g., [9]) and Z_i is the atomic number of element i.

Now we can derive ^{26}Al photon production rate of the Moon $L_{\leftmoon}$:

$$L_{\leftmoon} = 4\pi R_{\leftmoon}^2 \Delta r\, \rho_{\leftmoon}\, \epsilon_{\leftmoon} \frac{1 - \exp(-\alpha \Delta r)}{\alpha \Delta r}. \tag{2}$$

The factor of $[1 - \exp(-\alpha\Delta r)]/(\alpha\Delta r)$ comes from the slab approximation of self-absorption environment [10]. Therefore, we can determine the expected ^{26}Al photon flux from the Moon $F_{\leftmoon}$:

$$\begin{aligned} F_{\leftmoon} &= \frac{L_{\leftmoon}}{4\pi l_\mathrm{EM}^2} = \left(\frac{R_{\leftmoon}}{l_\mathrm{EM}}\right)^2 \Delta r\, \rho_{\leftmoon}\, \epsilon_{\leftmoon} \frac{1 - \exp(-\alpha\Delta r)}{\alpha \Delta r} \\ &\simeq 4.5 \times 10^{-6} \left(\frac{\Delta r}{33\ \mathrm{cm}}\right) \left(\frac{\epsilon_{\leftmoon}}{2.2 \times 10^{-3}\,/\mathrm{s/g}}\right)\ [\mathrm{ph/cm^2/s}], \end{aligned} \tag{3}$$

where $l_\mathrm{EM} = 3.844 \times 10^{10}$ cm: the distance (semi-major axis) from the Earth to the Moon [4]. Note that the Moon should be treated as a point source in the MeV domain due to the angular resolution

---

[1] This value is the volumetric mean radius of the Moon.

[2] We also estimated n_i using another chemical composition and its mass density $\rho_{\leftmoon} = 1.80\,\mathrm{g/cm^3}$ [6]. These different n_i and $\rho_{\leftmoon}$ have less impact on the final results, i.e. the expected ^{26}Al photon flux from the Moon. (cf., These data are compiled in TABLE I. of [7].)

of COSI. The angular resolution at 1.8 MeV is 1.5° FWHM [11], while the angular diameter of the Moon is about 0.5° [4]. According to the COSI (2-year suevey) line sensitivity at 1.8 MeV of 1.7×10^{-6} ph/cm^2/s [11], we expect that COSI will be able to detect the ^{26}Al gamma-ray signals from the Moon.

2.3 Aluminium-26 photon intensity from the main belt

We will derive an expected ^{26}Al gamma-ray signals from the MBAs here. Note that the derived quantity should be intensity—not be flux— since COSI cannot distinguish each asteroid in the main belt due to the angular resolution.

We treat each asteroid as a perfect sphere with a homogeneous density distribution in the same way as in Section 2.2. As parameters for MBAs, we only considered asteroid size (diameter) D, semi-major axis a, orbital inclination angle to the ecliptic i, and spectral type of asteroid j_s. It should be emphasized that inclination i is introduced to calculate the solid angle of the main belt measured from the Earth. Suppose that an asteroid is stationary at position A, located at a distance a from the Sun of the origin O, and tilted at an inclination i. Under this setup, we can define an angle $\theta_{\mathrm{OCA}} = \angle\mathrm{OCA}$, where point C represents the location of COSI. The distance CA is then a function of a and θ_{OCA}, or represented as $l_{\mathrm{CA}}(a,\, \theta_{\mathrm{OCA}})$[3]. For a fixed i, both the maximum and the minimum for θ_{OCA} are functions of a and i. Thus, the mean of l_{CA} regarding θ_{OCA} can also be expressed as the function with respect to a and i. Since it is enough for us to know the average value of l_{CA}, we do not need to consider θ_{OCA} as a variable, but as a function of a and i. We also assume that the main belt is symmetrically distributed around an axis perpendicular to the ecliptic plane centered on the Sun. Based on these assumptions, we will derive the total 1.8 MeV photon intensity from the MBAs in the following method.

For an asteroid with parameters $(D,\, a,\, i,\, j_s)$, we can formulate its ^{26}Al photon flux F_{A} in the same manner as Eq.(3):

$$F_{\mathrm{A}}(D,\, a,\, i,\, j_s) = \frac{1}{4} D^2 \left\langle \frac{1}{l_{\mathrm{CA}}^2} \right\rangle \Delta r\, \rho_{j_s}\, \epsilon_{\mathrm{MBA}} \frac{1 - \exp(-\alpha \Delta r)}{\alpha \Delta r}, \tag{4}$$

where $\langle l_{\mathrm{CA}}^{-2} \rangle$ is the average of l_{CA}^{-2} regarding θ_{OCA} (This is the function of a and i). For the CR penetration length Δr, using chemical composition of CI chondrites[4] [12], mass density of 2.0 g/cm^3[5], and the corresponding cross-section data from TALYS, we obtained $\Delta r \simeq 50$ cm. Here we assume the CR proton intensity I_{p} in the main belt is the same as I_{p} around the Moon.

To conduct a calculation on the total ^{26}Al flux from the MBAs, we considered the main belt distribution concerning the asteroid size D, the spectral type j_s, the semi-major axis a, and the inclination angle i. We overview the adopted distribution function below. As mentioned previously, we introduced i mainly to determine the solid angle of the main belt. Accordingly, we treat the distribution concerning i as a fraction of the MBAs with a representative value i_{r} assigned to each bin Δi, independent of D, j_s, a[6]: $w(i_{\mathrm{r}};\, \Delta i)$ such that $\sum_{i_{\mathrm{r}}} w = 1$. This assumption allows us to treat

---

[3] $l_{\mathrm{CA}}(a,\, \theta_{\mathrm{OCA}}) = \cos(\theta_{\mathrm{OCA}}) + \sqrt{\cos^2(\theta_{\mathrm{OCA}}) + a^2 - 1}$ in AU.

[4] Because of lacking data on chemical composition of asteroids, we use CI abundances instead. The CI chondrite is known as the ordinary meteorite, or the most primitive meteorite [12].

[5] We regard this value as the mean for density of MBAs (e.g., [13][14]).

[6] For the observational plots on semi-major axis a versus inclination i, see e.g., [15][16].

i separately from the other variables. We obtained data for w from [17] under the conditions. Let us denote the distribution function for MBAs as $\mathrm{d}^2N_{j_\mathrm{s}}(D,\,a)/\mathrm{d}D\mathrm{d}a$ for the other variables. We presume that $\mathrm{d}^2N_{j_\mathrm{s}}/\mathrm{d}D\mathrm{d}a$ is the following form:

$$\frac{\mathrm{d}^2N_{j_\mathrm{s}}(D,\,a)}{\mathrm{d}D\mathrm{d}a}=C\ f_{j_\mathrm{s}}(a)\,g(a)\,h(D), \tag{5}$$

where C is a normalization constant to meet Eq.(6), $f_{j_\mathrm{s}}(a)$ is the taxonomic distribution for each j_s, $g(a)$ is the spatial distribution, and $h(D)$ is the differential size distribution. $f_{j_\mathrm{s}}(a)$ is the fraction of the j_s-type asteroids by number as a function of a, and the data is taken from [13] with bin size of 0.02 AU (See, Fig.9. in [13]). Their analyses are based on data of the Sloan Digital Sky Survey (SDSS) [18], and the adopted data are limited to the size D of 5 km or larger to reduce biases (or selection effects). We also applied quantities stated in [13] to our calculations, such as j_s[7], ρ_{j_s}, and the main belt range definition (2.05 AU $\leq a \leq$ 3.27 AU). $g(a)$ is the spatial distribution by number taken from [19] with the same bin size as that of $f_{j_\mathrm{s}}(a)$. Therefore, $f_{j_\mathrm{s}}(a)g(a)$ provides the number distribution of each j_s-type asteroid, although the both distributions have biases in their data [20]. $h(D)$ have a broken power law form; $\propto D^{-2.3}$ for 0.4 km $\leq D \leq$ 5 km and $\propto D^{-4}$ for 5 km $\leq D \leq$ 40 km based on SDSS observations [18]; $\propto D^{-2.5}$ for 40 km $\leq D \leq$ 120 km and $\propto D^{-4}$ for 120 km $\leq D$ obtained from the broken power law fitting of the cumulative size distribution in [21] (See also [20]). It should be emphasized that we have little information on observationally motivated size distribution below sub-kilometer size. While asteroids are expected to exist down to sub meters, we need some extrapolations of $h(D)$ in order to treat these scales. These extrapolations may involve large uncertainties. Furthermore, even with extrapolation, there are limitations of the size D for $f_{j_\mathrm{s}}(a)$ and $g(a)$, rendering them no longer applicable to our calculations. Considering these factors, we set the lower limit of D as 1 km for $h(D)$. On the other hand, we put the upper limit of D to 332 km. Then, we excluded the four largest MBAs with $D >$ 400 km: (1) Ceres, (2) Pallas, (4) Vesta, and (10) Hygiea from $h(D)$. This exclusion is due to the discrepancy between the size of them estimated from [21] and from the recent observational data [22]. For these four asteroids, we conducted calculations individually[8]. The upper limit of 332 km is taken from the size of the fifth largest MBA: (704) Interamnia described in [22]. Now, all the distribution functions in Eq.(5) are introduced. Finally, we explain the normalization constant C. When normalizing $\mathrm{d}^2N_{j_\mathrm{s}}/\mathrm{d}D\mathrm{d}a$ by the total number of the MBAs, the influence of small asteroids becomes significant as D decreases. Since we impose limitations on the range of D, we instead normalize by the total mass of the main belt M_tot to enhance the influence of larger asteroids:

$$M_\mathrm{tot}-\sum_{k=1,\,2,\,4,\,10}M_{(k)}=\sum_{j_\mathrm{s}}\int\mathrm{d}D\mathrm{d}a\,\frac{\mathrm{d}^2N_{j_\mathrm{s}}(D,\,a)}{\mathrm{d}D\mathrm{d}a}\,\frac{4}{3}\pi\left(\frac{D}{2}\right)^3\,\rho_{j_\mathrm{s}}, \tag{6}$$

where $M_\mathrm{tot}=2.394\times10^{24}$ g [23] and $M_{(k)}$ is the mass of the four largest asteroids [22] (See, Table 1. in [22]). This is the condition that C needs to satisfy.

We can calculate the total flux of the MBAs F_MBAs

---

[7] Specifically, there are S, C, X, D, K, L, B, V, and A types. For density ρ_{j_s}, see Table 2 in [13] and reference there in.

[8] Since there is no information about their inclination i in [22], we obtained these data from [17].

3. Discussions

4. Summary

References

[1] K. Fuse and E. Anders, *Aluminum-26 in meteorites - VI. Achondrites*, **33** (1969) 653.

[2] C. Meyer, “Lunar sample compedium.” `https://curator.jsc.nasa.gov/lunar/lsc/index.cfm`, 2012.

[3] J. Wacker, J. Reeves et al., “Antarctic meteorite collection.” `https://curator.jsc.nasa.gov/antmet/us_clctn.cfm`, 2022.

[4] D.R. Williams, “Moon Fact Sheet.” `https://nssdc.gsfc.nasa.gov/planetary/factsheet/moonfact.html`, 2021.

[5] A.L. Turkevich, *Average Chemical Composition of the Lunar Surface*, *Moon* **8** (1973) 365.

[6] I.V. Moskalenko and T.A. Porter, *The Gamma-Ray Albedo of the Moon*, **670** (2007) 1467 [`0708.2742`].

[7] M. Ackermann, M. Ajello et al., *Measurement of the high-energy gamma-ray emission from the Moon with the Fermi Large Area Telescope*, **93** (2016) 082001 [`1604.03349`].

[8] A.J. Koning, S. Hilaire et al., *Talys-1.0*, in *International Conference on Nuclear Data for Science and Technology*, pp. 211–214, EDP Sciences, 2007.

[9] M.S. Longair, *High Energy Astrophysics* (2011).

[10] C.D. Dermer and G. Menon, *High Energy Radiation from Black Holes. Gamma Rays, Cosmic Rays, and Neutrinos* (2010).

[11] J. Tomsick, A. Zoglauer et al., *The Compton Spectrometer and Imager*, in *Bulletin of the American Astronomical Society*, vol. 51, p. 98, Sept., 2019, DOI [`1908.04334`].

[12] M. Asplund, A.M. Amarsi et al., *The chemical make-up of the Sun: A 2020 vision*, **653** (2021) A141 [`2105.01661`].

[13] F.E. DeMeo and B. Carry, *The taxonomic distribution of asteroids from multi-filter all-sky photometric surveys*, **226** (2013) 723 [`1307.2424`].

[14] I.V. Moskalenko, T.A. Porter et al., *A Celestial Gamma-Ray Foreground Due to the Albedo of Small Solar System Bodies and a Remote Probe of the Interstellar Cosmic-Ray Spectrum*, **681** (2008) 1708 [`0712.2015`].

[15] F.E. DeMeo and B. Carry, *Solar System evolution from compositional mapping of the asteroid belt*, **505** (2014) 629 [`1408.2787`].

[16] I.M.P. Center, "Distribution of the Minor Planets." https://minorplanetcenter.net/iau/lists/MPDistribution.html, 2015.

[17] I.M.P. Center, "MPC Database Search." https://minorplanetcenter.net/db_search, 2023.

[18] Ž. Ivezić, S. Tabachnik et al., *Solar System Objects Observed in the Sloan Digital Sky Survey Commissioning Data*, **122** (2001) 2749 [astro-ph/0105511].

[19] J.P. Laboratory, "Small-Body Database Query." https://ssd.jpl.nasa.gov/tools/sbdb_query.html, 2023.

[20] R. Jedicke, J. Larsen et al., *Observational Selection Effects in Asteroid Surveys*, in *Asteroids III*, pp. 71–87 (2002).

[21] W.F. Bottke, D.D. Durda et al., *The fossilized size distribution of the main asteroid belt*, **175** (2005) 111.

[22] P. Vernazza, M. Ferrais et al., *VLT/SPHERE imaging survey of the largest main-belt asteroids: Final results and synthesis*, **654** (2021) A56.

[23] E.V. Pitjeva and N.P. Pitjev, *Masses of the Main Asteroid Belt and the Kuiper Belt from the Motions of Planets and Spacecraft*, *Astronomy Letters* **44** (2018) 554 [1811.05191].